9-2013

Ground State of the Singly Ionized Oxygen Vacancy in Rutile TiO_2

A. T. Brant

Nancy C. Giles
Air Force Institute of Technology

M. A. R. Sarker
West Virginia University

S. Watauchi
University of Yamanashi

M. Nagao
University of Yamanashi

See next page for additional authors

Recommended Citation

Brant, A. T., et al. (2013). Ground state of the singly ionized oxygen vacancy in rutile TiO2. Journal of Applied Physics, 114(11),113702. https://doi.org/10.1063/1.4819805

Journal of Applied Physics

Ground state of the singly ionized oxygen vacancy in rutile TiO_2

Cite as: J. Appl. Phys. **114**, 113702 (2013); https://doi.org/10.1063/1.4819805
Submitted: 24 July 2013 . Accepted: 14 August 2013 . Published Online: 16 September 2013

A. T. Brant, N. C. Giles, Shan Yang (杨山), M. A. R. Sarker, S. Watauchi, M. Nagao, I. Tanaka, D. A. Tryk, A. Manivannan, and L. E. Halliburton

AIP Publishing

JOURNAL OF APPLIED PHYSICS **114**, 113702 (2013)

Ground state of the singly ionized oxygen vacancy in rutile TiO_2

A. T. Brant,[1] N. C. Giles,[1] Shan Yang (杨山),[2,a)] M. A. R. Sarker,[3,b)] S. Watauchi,[3] M. Nagao,[3] I. Tanaka,[3] D. A. Tryk,[4] A. Manivannan,[5] and L. E. Halliburton[2,c)]
[1]*Department of Engineering Physics, Air Force Institute of Technology, Wright-Patterson Air Force Base, Ohio 45433, USA*
[2]*Department of Physics, West Virginia University, Morgantown, West Virginia 26505, USA*
[3]*Center for Crystal Science and Technology, University of Yamanashi, 7-32 Miyamae, Kofu Yamanashi 400-8511, Japan*
[4]*Fuel Cell Nanomaterials Center, University of Yamanashi, 6-43 Miyamae-cho, Kofu, Yamanashi 400-0021, Japan*
[5]*National Energy Technology Laboratory, Morgantown, West Virginia 26507, USA*

(Received 24 July 2013; accepted 14 August 2013; published online 16 September 2013)

Results from electron paramagnetic resonance (EPR) and electron-nuclear double resonance (ENDOR) experiments are used to establish the model for the ground state of the singly ionized oxygen vacancy in the interior of bulk rutile TiO_2 crystals. Hyperfine from ^{47}Ti and ^{49}Ti nuclei show that the unpaired electron in this $S = 1/2$ defect is localized on one titanium ion adjacent to the oxygen vacancy (i.e., the spin is not shared by two titanium ions). These defects are formed at low temperature (~35 K) in as-grown oxidized crystals when sub-band-gap 442 nm laser light converts doubly ionized nonparamagnetic oxygen vacancies to the singly ionized paramagnetic charge state. The **g** matrix is obtained from EPR spectra and the ^{47}Ti and ^{49}Ti hyperfine and nuclear electric quadrupole matrices (**A** and **Q**) are obtained from ENDOR spectra. Principal values of the ^{47}Ti and ^{49}Ti hyperfine matrices are 64.54, 11.57, and 33.34 MHz. All the matrices have a principal axis along the [001] direction. In the basal plane, principal axes of the hyperfine and quadrupole matrices also coincide. The principal axes of the **g** matrix in the basal plane, however, deviate significantly from those of the **A** and **Q** matrices, thus indicating mixing of *d* orbitals due to the low symmetry at the Ti^{3+} ion site and participation of excited-state orbitals.
 [http://dx.doi.org/10.1063/1.4819805]

I. INTRODUCTION

The oxygen vacancy is an important intrinsic point defect in TiO_2 crystals, both rutile and anatase. Applications ranging from photocatalysts to memristors directly depend on the presence of these vacancies.[1–5] Interestingly, the oxygen vacancy in rutile-structured TiO_2, where bulk crystals provide more detailed information, exhibits unique behaviors that are not seen in other simple oxides such as ZnO and MgO.[6–8] For many years, much of the experimental information about oxygen vacancies in TiO_2 came indirectly from measurements of photocatalytic activity and from conductivity studies of reduced material. Then, early in 2009, Yang *et al.*[9] showed that doubly ionized oxygen vacancies ($S = 0$) were present in oxidized bulk rutile TiO_2 crystals and that the singly ionized ($S = 1/2$) and neutral ($S = 1$) charge states of these vacancies could be photoinduced at low temperature with laser light having a wavelength near the band edge. Using electron paramagnetic resonance (EPR), individual spectra from the $S = 1/2$ and $S = 1$ states of the oxygen vacancy were identified and the thermally induced conversion of $S = 1$ centers to $S = 1/2$ centers was established.[9,10] These results were verified by Brandão *et al.*[11] The $S = 1$ nature of the ground state of the neutral oxygen vacancy (where the spins of the two trapped electrons are aligned parallel) was unusual and its observation[9–11] was unexpected.

In the present paper, we use electron-nuclear double resonance (ENDOR) along with EPR to experimentally establish the ground-state model of the singly ionized ($S = 1/2$) oxygen vacancy in the interior of bulk rutile TiO_2 crystals. Significant concentrations of Fe^{3+} ions in our as-grown crystals allow large numbers of paramagnetic oxygen vacancies to be formed near 35 K when 442 nm laser light "pumps" electrons from the Fe^{3+} ions to "empty" nonparamagnetic oxygen vacancies. Easily detectable concentrations of oxygen vacancies are present in nearly all fully oxidized as-grown TiO_2 (rutile) crystals because they provide charge-compensation for residual Fe^{3+} and Cr^{3+} impurities substituting for Ti^{4+} ions.[9] Before illumination, these vacancies are in the doubly ionized (V_O^{++}) charge state, with no trapped electrons. Exposure at low temperature to laser light converts the vacancies to the singly ionized V_O^+ charge state (the $S = 1/2$ center with one trapped electron) and to the neutral V_O^0 charge state (the $S = 1$ center with two trapped electrons).

Development of a model for the ground state of the singly ionized (V_O^+) oxygen vacancy requires a detailed examination of the hyperfine structure found in the EPR spectra of this defect. The two relevant titanium isotopes are ^{47}Ti ($I = 5/2$, 7.44% abundant) and ^{49}Ti ($I = 7/2$, 5.41% abundant). These isotopes have similar small nuclear magnetic

a)Present address: Mechanical and Aerospace Engineering Department, Case Western Reserve University, Cleveland, Ohio 44106, USA.
b)Permanent address: Department of Physics, University of Rajshahi, Rajshahi 6205, Bangladesh.
c)Author to whom correspondence should be addressed. Electronic mail: larry.halliburton@mail.wvu.edu

moments; however, their nuclear electric quadrupole moments are large and different. As part of our study, we obtain the principal values and principal-axis directions of the **g** matrix from the angular dependence of the EPR spectra. We then continue to the main focus of our work, the analysis of hyperfine structure in the EPR and ENDOR spectra from the singly ionized oxygen vacancy. Angular dependence data allow us to determine the principal values and principal-axis directions of the ^{47}Ti and ^{49}Ti hyperfine and nuclear electric quadrupole matrices **A** and **Q**.

Our results show that the unpaired spin is localized primarily on one neighboring titanium ion. This resolves the fundamental question of how many titanium ions are directly involved in the electronic structure of the S = 1/2 oxygen vacancy. Previously, Yang *et al.*[9] had suggested that the unpaired spin was equally shared by two titanium neighbors while Brandão *et al.*[11] had indicated that two slightly inequivalent titanium neighbors shared the unpaired spin. The present definitive results provide direct experimental evidence that can be used by various computational groups conducting density-functional-theory (DFT) studies of oxygen vacancies in TiO_2. These DFT investigations are proving to be useful in understanding and predicting the fundamental behavior of point defects in this and similar materials.[12–24] The present study shows that the singly ionized oxygen vacancy can be readily viewed as a Ti^{3+} ion next to the perturbing vacancy. Thus, this defect is part of the larger family of Ti^{3+} ions often observed in TiO_2, which includes intrinsic and donor-bound polarons as well as oxygen vacancies near the surface.[25–33] The important distinguishing features of the EPR spectrum of the singly ionized oxygen vacancy in bulk rutile TiO_2 crystals, in contrast to the other Ti^{3+} centers, are larger negative g shifts and resolved ^{47,49}Ti hyperfine structure. [As a word of caution, we do not know if our results are relevant for singly ionized oxygen vacancies on the surface of rutile TiO_2 crystals. Future experimental and computational studies must explore this question.]

II. EXPERIMENTAL

The TiO_2 crystals used in the present study have the rutile structure and were grown by the four-mirror floating zone method[34] at the University of Yamanashi. Lattice constants[35,36] for rutile TiO_2 are $a = 4.5937$ Å, $c = 2.9587$ Å, and $u = 0.30478$ and the space group is $P4_2/mnm$ (D_{4h}^{14}). There are two slightly distorted TiO_6 octahedra in this tetragonal lattice. These two octahedra are equivalent, but are alternately elongated in [110] and [$\bar{1}$10] directions (they are related by a 90° rotation about the [001] direction). The six oxygen ions within an octahedron separate into two groups; four equatorial oxygens and two apical oxygens. At room temperature, the four equatorial oxygen ions are 1.9485 Å from the central Ti^{4+} ion and the two apical oxygen ions are 1.9800 Å from the Ti^{4+} ion.[35] Figure 1(a) shows one of the two TiO_6 octahedra along with its eight nearest-neighbor Ti^{4+} ions. A titanium ion has six oxygen neighbors in this lattice, but an oxygen ion has only three titanium neighbors. In direct analogy to the two equivalent TiO_6 octahedra, the oxygen ion and its three titanium neighbors also have two

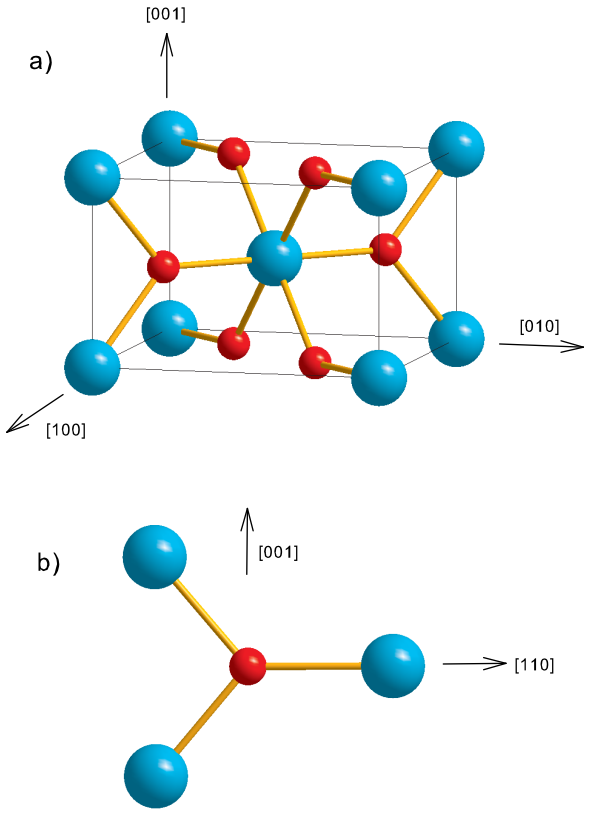

FIG. 1. (a) Schematic representation of one of the two equivalent TiO_6 octahedra in the TiO_2 (rutile) lattice. Titanium ions are blue and oxygen ions are red. (b) An oxygen ion and its three nearest titanium neighbors.

equivalent orientations. These Ti_3O "units" lie in either a ($\bar{1}$10) plane, as illustrated in Fig. 1(b), or in a (110) plane. In Fig. 1(b), the two titanium ions along the [001] direction are equivalent while the third titanium along the [110] direction is slightly farther from the oxygen ion.

The as-grown TiO_2 crystals selected for our investigation contained more than 100 ppm of Fe^{3+} ions substituting for Ti^{4+} ions (determined with EPR). This gave the crystals an orange color. The observation of Fe^{3+} impurities in the as-grown crystals implies that doubly ionized oxygen vacancies must also be present (i.e., nonlocal charge compensation for two substitutional Fe^{3+} ions is provided by one doubly ionized oxygen vacancy). Thus, these specific crystals are well-suited for photoinduced EPR studies of isolated paramagnetic oxygen vacancies. Although not relevant to our study, large concentrations of oxygen vacancies, considerably beyond that needed for charge compensation of trivalent impurities, can easily be produced in rutile TiO_2 crystals during reducing treatments at elevated temperatures.

The EPR data were taken with a Bruker EMX spectrometer and the ENDOR data were taken with a Bruker Elexsys E-500 spectrometer. These spectrometers operated near 9.4 and 9.5 GHz, respectively. During the ENDOR experiments, the rf was frequency-modulated at 20 kHz (thus giving first-derivative ENDOR signals). An Oxford Instruments helium-gas-flow system maintained the sample temperature near 35 K for the EPR measurements and near 21 K for the ENDOR measurements. Proton NMR gaussmeters were used to measure the static magnetic field and a small Cr-doped

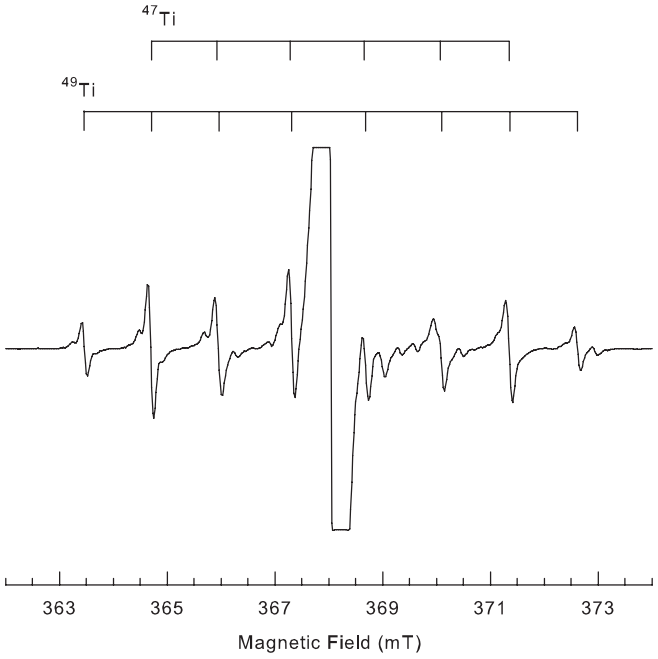

FIG. 2. Photoinduced EPR spectrum from the singly ionized oxygen vacancy taken at 35 K after exposure at this temperature to 442 nm laser light. The magnetic field is in the [001] direction and the microwave frequency is 9.396 GHz. Stick diagrams identify ^{47}Ti and ^{49}Ti hyperfine lines.

MgO crystal was used to correct for the difference in magnetic field between the sample position and the gaussmeter probe (the isotropic g value for Cr^{3+} in MgO is 1.9800). Approximately 5 mW of 442 nm light from a He-Cd laser was incident on the sample during the low-temperature illuminations. Narrow slots in the side of the Bruker high-sensitivity circular microwave cavity provided optical access to the sample during the EPR experiments. The Bruker cylindrical ENDOR cavity did not have slots for optical access. In the ENDOR experiments, the sample was attached to the end of a vertical solid glass rod (high purity silica) and the rod then served as a light pipe for the laser light.

III. EPR RESULTS

Figures 2 and 3 show representative EPR spectra from the singly ionized oxygen vacancy ($S = 1/2$) in an oxidized TiO_2 (rutile) crystal. These data were taken at 35 K after illumination at this temperature with 442 nm laser light. The magnetic field is along the [001] direction in Fig. 2 and along the [100] direction in Fig. 3. Three intense primary lines, at 368.08 mT in Fig. 2 and at 343.01 and 349.86 mT in Fig. 3, are off-scale and are due to those oxygen vacancies having no participating ^{47}Ti or ^{49}Ti nuclei. Surrounding the primary lines are well-resolved sets of less intense hyperfine lines due to ^{47}Ti and ^{49}Ti nuclei. Stick diagrams above the spectra identify the ^{47}Ti and ^{49}Ti lines associated with each primary line. Because of their very similar nuclear magnetic moments, the six hyperfine lines from ^{47}Ti nuclei overlap the inner six lines from ^{49}Ti nuclei (this gives eight observable hyperfine lines with the outer two being less intense). In Fig. 2, the hyperfine lines are separated by approximately 1.31 mT. For the [100] direction of field in Fig. 3, hyperfine lines in the higher-field set are separated by 1.99 mT and lines in the lower-field set are separated by 1.39 mT. The prominent line at 345.75 mT near the middle of the spectrum

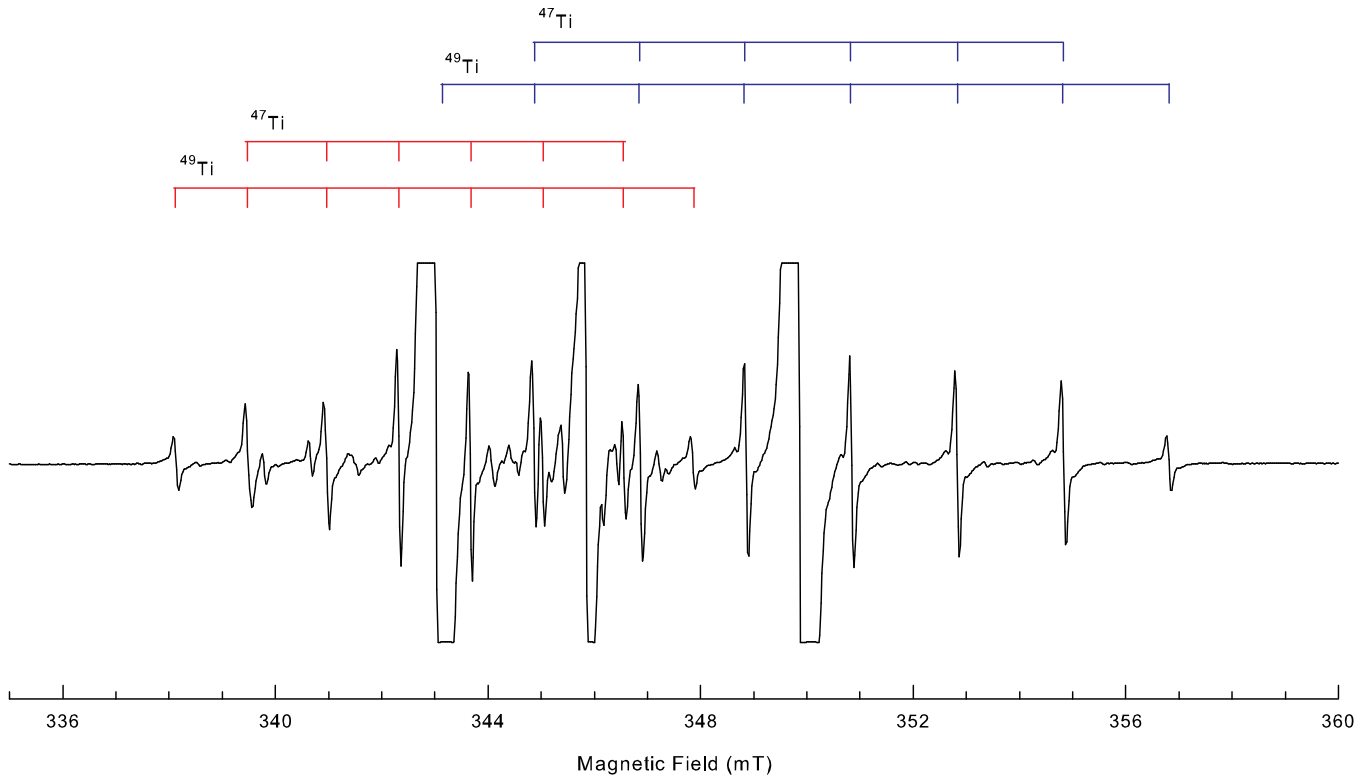

FIG. 3. Photoinduced EPR spectrum from the singly ionized oxygen vacancy taken at 35 K after exposure at this temperature to 442 nm laser light. The magnetic field is in the [100] direction and the microwave frequency is 9.397 GHz. There are two magnetically inequivalent orientations of the defect for this direction of magnetic field. Stick diagrams identify the ^{47}Ti and ^{49}Ti hyperfine lines (red for lower-field set and blue for higher-field set).

in Fig. 3 is due to the Ti^{3+}-Si^{4+} centers initially reported by Yang *et al.*[9]

A. Determination of the g matrix

The complete angular dependence of the primary (I = 0) EPR lines for the S = 1/2 oxygen vacancy is shown in Fig. 4. Data were taken every 10° when rotating from [001] to [100] and from [001] to [110] and every 15° when rotating from [110] to $[1\bar{1}0]$. As shown in Fig. 4, the spectrum separates into two branches for rotation in the (010) plane and $(1\bar{1}0)$ plane and into four branches for rotation in the (001) plane. This establishes that there are four magnetically inequivalent, but crystallographically equivalent, orientations of the singly ionized oxygen vacancy. Defect sites (or orientations) are magnetically inequivalent when the magnetic field makes different projections on the **g**-matrix principal-axis directions. Principal values of the **g** matrix are the same for these magnetically inequivalent sites, but the principal-axis coordinate systems are rotated relative to each other, according to the symmetry elements of the crystal. For the S = 1/2 oxygen vacancy, the four orientations are magnetically equivalent when the magnetic field is along the [001] direction. There are two inequivalent sets (each doubly degenerate) when the magnetic field is along the [100] or [110] directions.

The **g** matrix of the S = 1/2 oxygen vacancy is obtained from the angular dependence of the primary (I = 0) lines in the EPR spectrum. A spin Hamiltonian, containing only the electron Zeeman term, is used

$$\mathbf{H} = \beta \mathbf{S} \cdot \mathbf{g} \cdot \mathbf{B}. \quad (1)$$

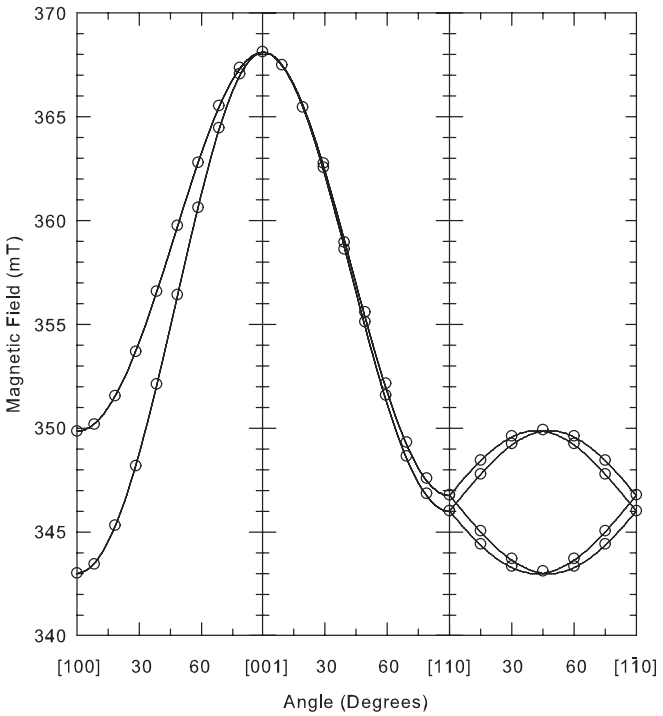

FIG. 4. Angular dependence of the **g** matrix. Data from the primary (I = 0) EPR lines are shown for three high-symmetry planes of the crystal. The discrete points are experimental results and the solid curves are computer-generated using the **g** matrix parameters in Table I.

A "turning point" occurs in Fig. 4 when the magnetic field is along the [001] direction. Thus, one of the principal axes of the **g** matrix must be along this direction. The other two principal axes must be in the basal plane with their directions specified by one angle. The four parameters (three principal values and one angle) required to describe the **g** matrix are determined by fitting the experimental data points in Fig. 4. Table I contains the "best-fit" set of parameters for the **g** matrix. The solid curves in Fig. 4 were then computer-generated using these final values. The results in Table I for the **g** matrix are similar to the previously reported values[10,11]

The principal axes associated with the 1.9572 and 1.9187 principal values are in the basal plane and deviate only 3.1° from ⟨100⟩ directions. Although small, this angle is significant and it leads to a question when relating the principal-axis directions, and their corresponding principal values, to a defect located within a specific TiO_6 octahedron (the problem occurs because rutile crystals contain two equivalent TiO_6 units rotated by 90° about the [001] direction). In particular, the experimental data in Fig. 4 do not determine which basal-plane principal value (1.9572 or 1.9187) has its principal-axis closest to the direction from the central Ti ion to an apical oxygen neighbor. Similar questions arise in Secs. IV and V when directions of the principal axes of the hyperfine and nuclear electric quadrupole matrices in the basal plane are related to a specific Ti^{3+} site.

B. Hyperfine from ^{47}Ti and ^{49}Ti nuclei

The [001] and [100] EPR spectra in Figs. 2 and 3 answer the important question of how many titanium ions (one, two, or three) contribute to the observed hyperfine pattern.

TABLE I. Spin-Hamiltonian parameters for the S = 1/2 singly ionized oxygen vacancy in TiO_2 (rutile) crystals. The **A** and **Q** matrices are obtained from ENDOR data (units for the principal values are MHz). Directions of the principal axes for g_1, g_2, A_1, A_2, Q_1, and Q_2 are in the (001) plane. Two choices arise when relating these principal-axis directions to a specific TiO_6 unit. The estimated error is ±0.0003 for the principal *g* values, ±0.03 MHz for the principal A values, ±0.003 MHz for the principal Q values, and ±1° for the directions of the principal axes.

	Principal value	Principal-axis direction
	g matrix	
g_1	1.9572	41.9° from [110] toward [010]
g_2	1.9187	41.9° from [$\bar{1}$10] toward [$\bar{1}$00]
g_3	1.8239	[001]
	A hyperfine matrix for both ^{47}Ti and ^{49}Ti	
A_1	64.54	10.4° from [110] toward [100]
A_2	11.57	10.4° from [$\bar{1}$10] toward [010]
A_3	33.34	[001]
	Q nuclear electric quadrupole matrix for ^{47}Ti	
Q_1	−2.309	11.4° from [110] toward [100]
Q_2	1.222	11.4° from [$\bar{1}$10] toward [010]
Q_3	1.087	[001]
	Q nuclear electric quadrupole matrix for ^{49}Ti	
Q_1	−0.910	11.4° from [110] toward [100]
Q_2	0.482	11.4° from [$\bar{1}$10] toward [010]
Q_3	0.428	[001]

These two spectra clearly show that only one set of eight Ti hyperfine lines surrounds each primary (I = 0) line. This means that the unpaired spin is not distributed in a significantly unequal manner on two or three titanium ions. If that were the case, each primary I = 0 line in these EPR spectra would be surrounded by two or three sets of eight hyperfine lines, given the low abundances of the ^{47}Ti and ^{49}Ti nuclei. This leaves two possibilities: either the unpaired spin is shared equally, or almost equally, by two or three of the neighboring titanium ions or it is localized to a very large extent on one titanium ion. Both possibilities would produce only one easily observed set of eight lines around each primary I = 0 line. We used the ratio of the intensity of a hyperfine line to the intensity of the corresponding central line in Fig. 3 to decide which possibility is correct. In Fig. 3, a careful measurement of the high-field primary line, near 349.86 mT, and the highest-field ^{49}Ti line, at 356.80 mT, gives an experimental value of 120 for the ratio of their intensities. This compares favorably with the predicted value of 129 if only one titanium ion is involved (the predicted value for this ratio would be approximately 60 if the unpaired spin were shared equally by two titanium ions and even smaller if the spin were shared equally by three titanium ions). Also, additional low-intensity lines would be present in the EPR spectra if two or more nuclei are involved. In Fig. 3, weak lines would occur in the magnetic field region above the ^{49}Ti line at 356.80 mT and below the ^{49}Ti line at 338.13 mT if two or three titanium ions equally share the unpaired spin and all have a magnetic nucleus. These extra outer lines arise when one oxygen vacancy has more than one neighboring ^{47,49}Ti magnetic nucleus contributing to its hyperfine pattern. The intensities of these "extra" lines would be determined by a statistical distribution based on the natural abundances of the participating magnetic nuclei. We did not observe these extra lines (our signal-to-noise ratio was sufficient to easily detect these small lines, had they been present). Thus, we conclude that the unpaired spin in the singly ionized oxygen vacancy is to a very large extent localized on one neighboring titanium ion (i.e., the defect consists of a Ti^{3+} ion adjacent to the oxygen vacancy).

Despite the simple appearance of the ^{47}Ti and ^{49}Ti EPR hyperfine lines in Figs. 2 and 3, they are not well-resolved for many other directions of magnetic field. Also, for some directions of field, hyperfine lines within a set are not equally spaced, thus indicating a significant nuclear electric quadrupole effect. Direct evidence that the nuclear electric quadrupole interaction is important is provided by the EPR spectrum in Fig. 5. These data were taken at 35 K with the magnetic field rotated 50° from the [001] direction toward the [100] direction. The spectrum shows the highest-field hyperfine lines associated with the upper branch in the left panel of Fig. 4. It is clear in Fig. 5 that the ^{47}Ti and ^{49}Ti hyperfine lines do not overlap. In the absence of a quadrupole interaction, EPR hyperfine lines from the two Ti isotopes are expected to coincide because their nuclear magnetic moments are nearly identical. However, a substantial nuclear electric quadrupole effect can change this expectation. The electric quadrupole moments of the two isotopes[37] are different (0.29 barns for ^{47}Ti and 0.24 barns for ^{49}Ti) and the

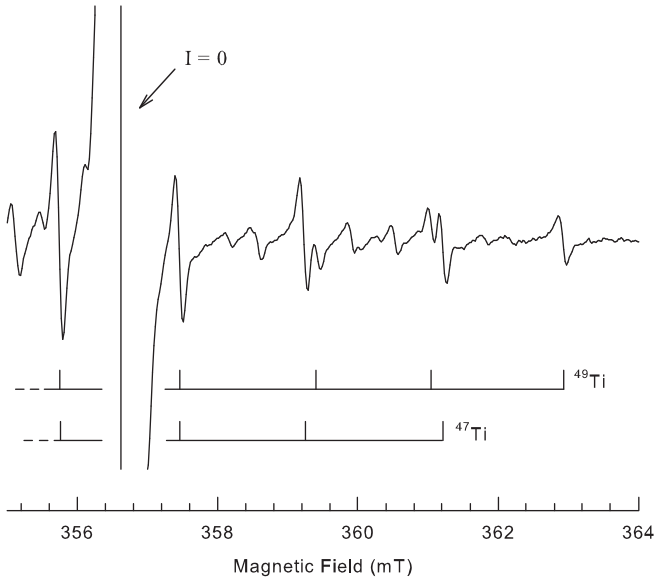

FIG. 5. Illustration of relative shifts in the positions of hyperfine lines due to the large nuclear electric quadrupole interaction. Shown are high-field hyperfine lines associated with the upper EPR branch in the left panel of Fig. 4. These data were taken with the magnetic field oriented 50° from the [001] direction toward the [100] direction.

nuclear spins are different (I = 5/2 and I = 7/2). Together, these factors produce easily observed relative shifts of the ^{47}Ti and ^{49}Ti hyperfine lines when the electric field gradient at the nuclei is sufficiently large, as demonstrated in Fig. 5. Rinneberg and Weil[38] have reported this effect in the EPR spectra from Ti^{3+} ions in single crystals of SiO_2 (quartz).

The large number of overlapping hyperfine lines as well as the shifting of lines, variations in their intensity, and the introduction of forbidden lines caused by the nuclear quadrupole effect make it difficult to extract a final set of hyperfine and nuclear electric quadrupole parameters from EPR data alone (this task is best accomplished using higher-resolution ENDOR data, as described in Sec. IV). A preliminary, and useful, set of hyperfine parameters can, however, be determined from the EPR angular-dependence data. The outermost hyperfine lines around each primary I = 0 line are due to ^{49}Ti nuclei and the lowest and highest of these lines can be clearly observed for many directions of magnetic field. Positions of these lowest and highest ^{49}Ti lines were measured during rotations of the field from [001] to [100], [001] to [110], and [110] to $[1\bar{1}0]$. The outer ^{49}Ti lines showed no splitting for any directions in these three rotation planes, thus demonstrating that the [001] direction is a principal axis of the hyperfine matrix (the other two principal axes of the hyperfine matrix must be in the basal plane). This is the same behavior previously observed for the **g** matrix. Our data, i.e., the outer ^{49}Ti EPR lines from the three planes, were then "fit" using a spin-Hamiltonian containing electron Zeeman and hyperfine terms. The **g** matrix parameters were held constant at the values given in Table I. The resulting four hyperfine parameters, three principal values and one basal-plane angle, were 64.9, 11.7, and 33.6 MHz and 10.7°. Here, the principal axis associated with the 33.6 MHZ principal value is along the [001] direction and the principal axis associated with the 64.9 MHz principal value is 10.7° from

[110] toward [100]. These results, obtained only from EPR data, are very similar to the final parameters resulting from the more complete analysis of ENDOR data (see Sec. IV and Table I). As an illustration of the experimental data used in this fitting process, Fig. 6 includes the discrete ^{49}Ti experimental points representing the highest-field line from one set of hyperfine lines and the lowest-field line from the other set when the magnetic field is rotated from [001] to [100]. These two sets correspond to the two branches seen in the left panel of Fig. 4. The solid curves in Fig. 6, representing the eight allowed ^{49}Ti hyperfine lines for each set, were computer-generated using the final values of the ^{49}Ti parameters listed in Table I. The two primary $I = 0$ central lines are not included in Fig. 6.

IV. ENDOR RESULTS

With its higher resolution and simpler patterns, ENDOR is used to determine a final set of hyperfine and nuclear electric quadrupole parameters for the singly ionized oxygen vacancy ($S = 1/2$) in rutile TiO_2. Figure 7 shows two ENDOR spectra taken at 21 K with the magnetic field along the [001] direction. Lines from ^{49}Ti nuclei are labeled with an asterisk and lines from ^{47}Ti nuclei are labeled with numbers. Figure 8 is the (M_S,m_I) energy level scheme appropriate for a ^{47}Ti nucleus in this oxygen-vacancy defect when the magnetic field is in the [001] direction. A similar energy-level diagram for a ^{49}Ti nucleus is not shown. In Fig. 8, EPR transitions (in red) obey $\Delta M_S = \pm 1$, $\Delta m_I = 0$ selection rules and are labeled with letters while ENDOR transitions (in blue) obey $\Delta M_S = 0$, $\Delta m_I = \pm 1$ selection rules and are labeled with numbers. The labeling of the ENDOR transitions in Fig. 8 is consistent with the labeling of the experimentally observed ^{47}Ti ENDOR lines in Fig. 7.

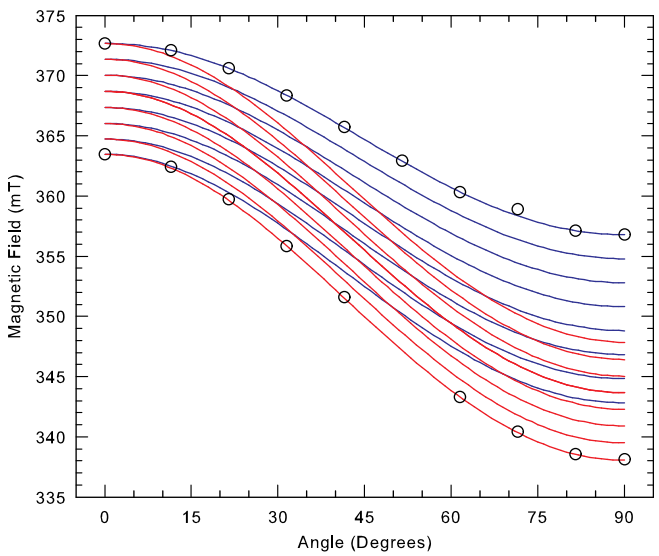

FIG. 6. Angular dependence of the ^{49}Ti EPR hyperfine lines when the magnetic field is rotated from the [001] direction to the [100] direction. There are two sets of lines (in red and blue) corresponding to the two branches in Fig. 4. Central $I = 0$ lines are not included. The discrete points are experimental results and the solid curves are computer-generated using parameters from Table I for the **g** and the ^{49}Ti hyperfine and quadrupole matrices.

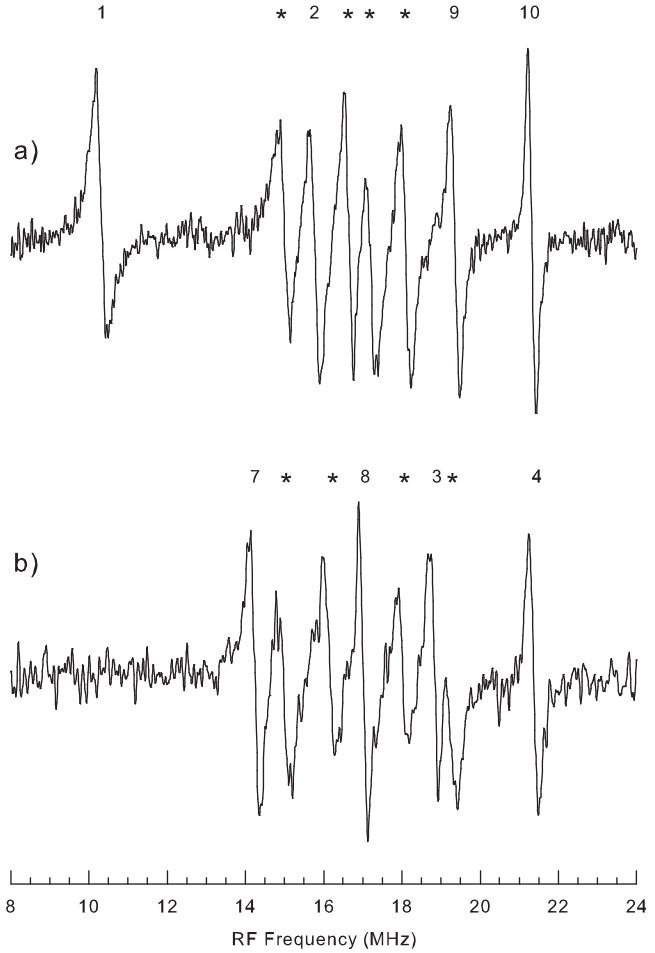

FIG. 7. ENDOR spectra from the singly ionized oxygen vacancy taken at 21 K after exposure to 442 nm laser light. The magnetic field is in the [001] direction. Spectra (a) and (b) were taken while sitting on different EPR lines, as described in the text. The ^{47}Ti lines are numbered and correspond to the labels in Fig. 8. The ^{49}Ti lines are identified by asterisks.

The ENDOR spectrum in Fig. 7(a) was acquired at a static magnetic field of 369.66 mT and a microwave frequency of 9.4918 GHz, corresponding to the third hyperfine line (i.e., the second ^{47}Ti line) up from the low-field end in Fig. 2. This is the EPR transition labeled b in Fig. 8. The magnetic field for this line in Fig. 2 is different than the magnetic field in the ENDOR experiment because the two microwave cavities had slightly different resonant frequencies. Since all of the EPR hyperfine lines in Fig. 2 are well-resolved, only the four ENDOR lines labeled 1, 2, 9, and 10 in Fig. 8 are expected from ^{47}Ti nuclei when monitoring transition b. Experiment provides verification of this expectation since only four ENDOR lines associated with ^{47}Ti nuclei are seen in Fig. 7(a). Similarly, four ENDOR lines from the ^{49}Ti nuclei are expected, and observed, in Fig. 7(a). Keeping the magnetic field along the [001] direction but fixing its magnitude at transition d in Fig. 8 (i.e., a different EPR line) gave the ENDOR spectrum shown in Fig. 7(b). This spectrum was acquired at a static magnetic field of 372.41 mT and a microwave frequency of 9.4919 GHz, corresponding to the fifth hyperfine line up from the low-field end in Fig. 2. Again, there are four ENDOR lines from ^{47}Ti nuclei and four lines from ^{49}Ti nuclei. It is clear from the

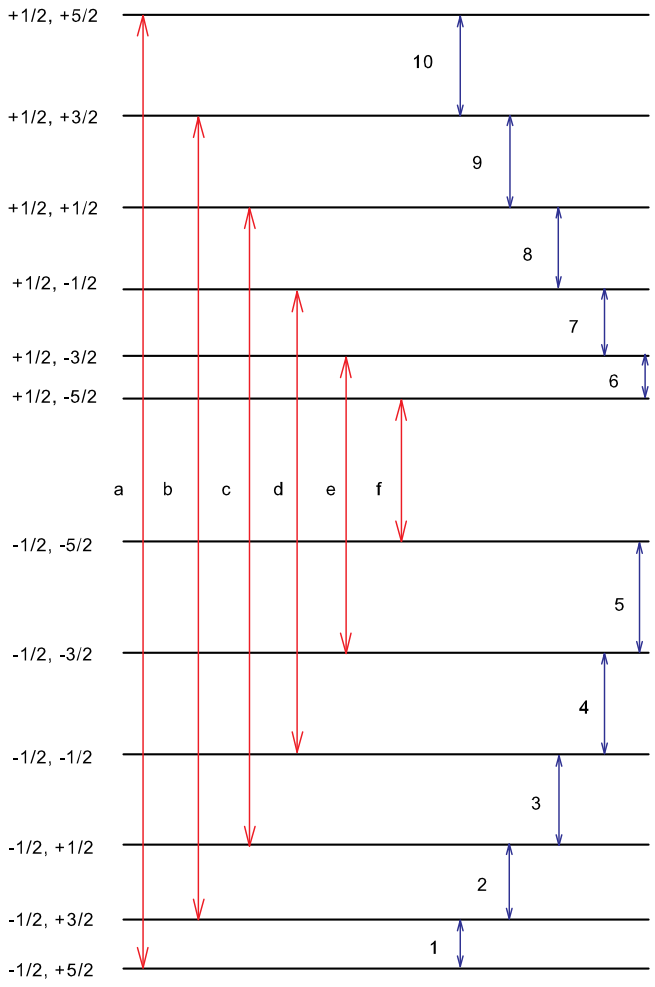

FIG. 8. The relative energy levels for an S = 1/2, I = 5/2 spin system. This diagram corresponds to the singly ionized oxygen vacancy with hyperfine from one ^{47}Ti nucleus when the magnetic field is along the [001] direction. Levels are labeled with their M_S and m_I values. Allowed EPR transitions are red and ENDOR transitions are blue.

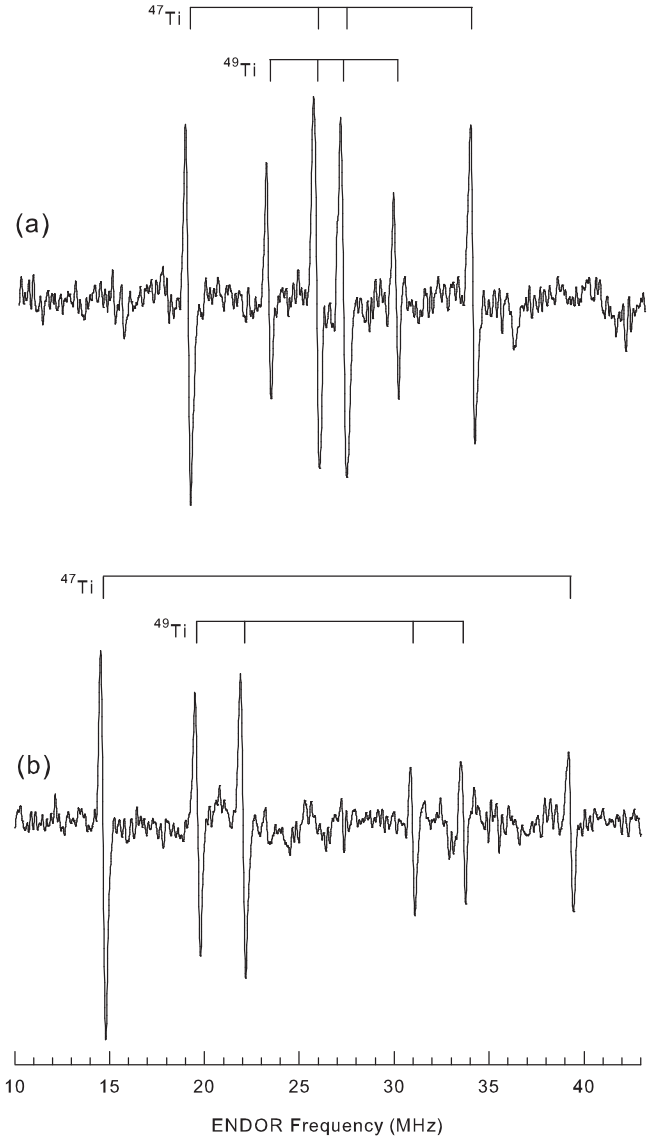

FIG. 9. ENDOR spectra from the singly ionized oxygen vacancy taken at 21 K after exposure to 442 nm laser light. The magnetic field is in the [100] direction. Spectra (a) and (b) were taken while sitting on different EPR lines, as described in the text. Stick diagrams assign individual lines to either ^{47}Ti or ^{49}Ti nuclei.

ENDOR spectra in Fig. 7 that the hyperfine interactions dominate and the nuclear electric quadrupole interactions are larger than the nuclear Zeeman interactions. In particular, the widely separated lines in the ENDOR spectra in Fig. 7 provide evidence that a significant nuclear electric quadrupole interaction is present.

Figure 9 shows ENDOR spectra taken while "sitting" on hyperfine lines in the high-field portion of the [100] EPR spectrum shown in Fig. 3. The ENDOR spectrum in Fig. 9(a) was acquired at a static magnetic field of 352.41 mT and a microwave frequency of 9.4944 GHz, which corresponds to the third ^{47}Ti hyperfine line up from the low-field end in the set of lines surrounding the upper I = 0 line in Fig. 3. In Fig. 9(b), the ENDOR spectrum was acquired at a static magnetic field of 358.36 mT and a microwave frequency of 9.4942 GHz, corresponding to the highest field ^{47}Ti hyperfine line in the set of lines surrounding the upper I = 0 line in Fig. 3. As expected for these specific EPR lines, there are four lines in each spectrum in Fig. 9 from ^{49}Ti nuclei. There are also four lines from ^{47}Ti nuclei in Fig. 9(a), but two of these ^{47}Ti lines directly overlap two of the ^{49}Ti lines. Only two lines from ^{47}Ti nuclei appear in Fig. 9(b) because this ENDOR spectrum was obtained while monitoring the outermost ^{47}Ti EPR hyperfine line.

The **A** and **Q** matrices (for the ^{47}Ti nuclei) are obtained from the angular dependence of the ENDOR spectra. We focus on ^{47}Ti because of its larger abundance and smaller I value and use a spin Hamiltonian with electron Zeeman, hyperfine, quadrupole, and nuclear Zeeman terms

$$H = \beta \mathbf{S}\cdot\mathbf{g}\cdot\mathbf{B} + \mathbf{I}\cdot\mathbf{A}\cdot\mathbf{S} + \mathbf{I}\cdot\mathbf{Q}\cdot\mathbf{I} - g_N\beta_N\mathbf{I}\cdot\mathbf{B}. \quad (2)$$

From the analysis of the EPR hyperfine lines in Sec. III B, we found that one of the principal axes of the hyperfine matrix **A** was along the [001] direction. This leaves four parameters (three principal values and one angle) to be determined for this matrix. The nuclear electric quadrupole matrix **Q** is

traceless ($Q_{xx} + Q_{yy} + Q_{zz} = 0$) with the principal value Q_{zz} defined as $e^2qQ/[2I(2I–1]$, where eq is the electric field gradient and Q is the nuclear quadrupole moment. One principal axis of the quadrupole matrix **Q** is also along the [001] direction and only three parameters (two principal values and one angle) must be determined from experiment for this matrix.

Sets of ^{47}Ti ENDOR data were accumulated for five different orientations of the oxygen vacancy defect relative to the magnetic field. These include one set with the magnetic field along the [001] direction, two sets with the magnetic field along the [100] direction (the upper and lower branches in Fig. 4), one set with the magnetic field along the [110] direction (the upper branch in Fig. 4), and one set with the magnetic field rotated 60° from [001] toward [100] (the upper branch in Fig. 4). Each set contained ENDOR spectra associated with different m_I values, i.e., ENDOR spectra were acquired while sitting on different hyperfine lines within the particular EPR spectrum. Three of these sets of ^{47}Ti ENDOR data are illustrated by the discrete points shown in Fig. 10. Together, the five sets of ENDOR data provided 44 lines from ^{47}Ti nuclei for use in a fitting program to determine final values of the seven ^{47}Ti parameters. After converting the spin Hamiltonian in Eq. (2) to a 12×12 matrix, exact diagonalizations were performed during an iterative computer fitting procedure and the resulting "best-fit" ^{47}Ti parameters are listed in Table I. The solid curves in Fig. 10 were then generated using these final values of the parameters. The final **A** and **Q** parameters for the ^{49}Ti nuclei in Table I were not determined independently. Because of the nearly identical magnetic moments for the two nuclei, the ^{49}Ti **A** principal values are taken to be the same as the ^{47}Ti **A** principal values. The ^{49}Ti **Q** principal values are obtained by multiplying the ^{47}Ti **Q** values by 0.3941 (this factor emerges from the ratio of Q/[2I(2I–1] for the two isotopes where the nuclear electric quadrupole moments are $^{47}Q = 0.29$ barns and $^{49}Q = 0.24$ barns). Following the work of earlier investigators,[38,39] we assign positive signs to the principal values of the hyperfine **A** matrix in Table I. This, in turn, fixes the signs of the quadrupole principal values because the relative signs of the **A** and **Q** parameters are determined in ENDOR experiments. As previously described in Sec. III A, a question arises when attempting to relate principal-axis directions to the positions of oxygen ions around a Ti^{3+} ion. The basal-plane principal-axis directions listed in Table I may apply to either one of the two equivalent, but differently oriented, TiO_6 octahrdra in this lattice.

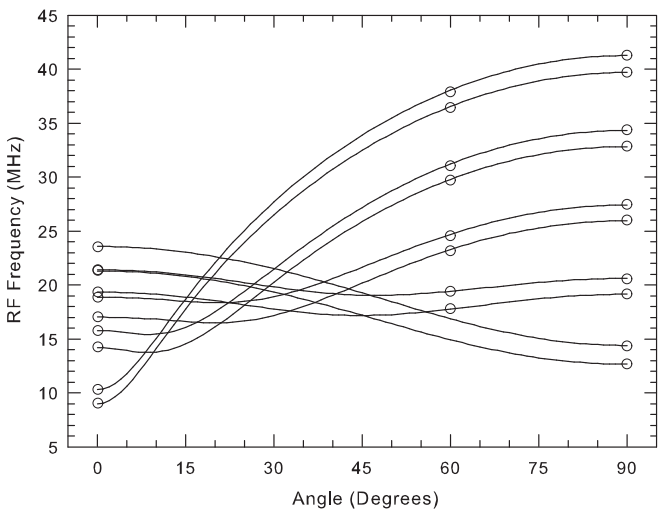

FIG. 10. Angular dependence of the ^{47}Ti ENDOR spectrum for rotation of the magnetic field from [001] to [100]. These data were taken when sitting on EPR hyperfine lines associated with the upper branch in Fig. 4. The discrete points are experimental results and the solid curves are computer-generated using parameters in Table I for the ^{47}Ti hyperfine and quadrupole matrices.

V. DISCUSSION

An oxygen vacancy in a rutile TiO_2 crystal has three neighboring titanium ions. Until the present investigation, it was not known how the unpaired spin density was distributed amongst these titanium ions when one electron was trapped by the vacancy. We have now shown with EPR and ENDOR data that the unpaired spin in this $S = 1/2$ defect is localized primarily on only one titanium ion. Specifically, the electronic ground state of the singly ionized oxygen vacancy is best described as a Ti^{3+} ion next to an "empty" vacancy. The important question then becomes where the Ti^{3+} ion is located relative to the oxygen vacancy. There are only two possibilities. As described in Sec. II and shown in Fig. 1(a), a titanium ion in rutile has four equatorial oxygen neighbors and two apical neighbors. Thus, the oxygen vacancy may be at an equatorial position or at an apical position next to the Ti^{3+} ion.

Fortunately, the results of Yang[10] and Brandão *et al.*[11] for the $S = 1$ charge state of the neutral oxygen vacancy in rutile TiO_2 suggest an answer to this question of the position of the vacancy in the $S = 1/2$ defect. These investigators used the following spin-Hamiltonian, with an electron Zeeman term and a fine structure (i.e., spin-spin) term, to describe the $S = 1$ defect.

$$H = \beta \mathbf{S} \cdot \mathbf{g} \cdot \mathbf{B} + \mathbf{S} \cdot \mathbf{D} \cdot \mathbf{S}. \quad (3)$$

Here, the **D** matrix represents a magnetic dipole-dipole interaction between the two unpaired spins, one at each Ti^{3+} site. The largest (i.e., unique) principal value of this traceless matrix has its principal axis along the [001] direction.[10,11] The principal values[10] of the **D** matrix are 291.5, 168.5, and −460.0 MHz. In a simple point dipole-dipole model, these values predict a distance of approximately 4.67 Å between the two unpaired spins. Here, we use the expression $D_{zz} = -\mu_0 g^2 \beta^2 / 4\pi h R^3$ adapted from Abraham *et al.*[40] This translates to $R^3 D_{zz} \approx 4.68 \times 10^4$ if g is taken to be 1.9, R has units of Å, and D_{zz} has units of MHz. For comparison, the separation of two titanium ions along the [001] direction in the unperturbed lattice is 2.96 Å at room temperature. Point-dipole approximations often overestimate separation distances for $S = 1$ biradicals.[41] These experimental results for **D**, i.e., the magnitudes of the principal values and the directions of the principal axes, strongly suggest that the $S = 1$ oxygen vacancy consists of two adjacent Ti^{3+} ions aligned along the [001] direction with the oxygen vacancy at the nearest equatorial oxygen site between the two Ti^{3+} ions, i.e., the oxygen

vacancy is equidistant from the two Ti^{3+} ions. This model of the $S = 1$ oxygen vacancy is easily visualized with the aid of Fig. 1(b).

As shown by the earlier investigators,[9–11] the two defects represented by the $S = 1/2$ and $S = 1$ charge states of the oxygen vacancy are closely related. Significant concentrations of both defects can be formed during exposure to laser light at 35 K. Then, when the light is removed and the crystal is kept at this temperature, the $S = 1$ defects quickly convert to $S = 1/2$ defects. One of the two trapped electrons is thermally released from an $S = 1$ defect and an $S = 1/2$ defect is formed. This conversion of an oxygen vacancy from the two-trapped-electron state to the one-trapped-electron state is expected to occur without significant changes in the surrounding lattice relaxation and without a major redistribution of the remaining unpaired spin density. In other words, the remaining electron should not hop or tunnel from one of the two titanium ions along the [001] direction to the third inequivalent titanium ion along the [110] direction during the $S = 1$ to $S = 1/2$ thermal conversion process. Specifically, after losing one electron, the remaining electron and the oxygen vacancy (which together now form the $S = 1/2$ defect) are expected to still be near the positions they initially had in the $S = 1$ defect. The model of the $S = 1$ defect and the expected behavior of its constituents during the thermal conversion process strongly suggests that the oxygen vacancy is located at an equatorial position next to the Ti^{3+} ion in the $S = 1/2$ oxygen vacancy. Although we believe that it is much less likely, we cannot completely rule out a model for the $S = 1/2$ oxygen vacancy that has the Ti^{3+} ion along a $\langle 110 \rangle$ direction from the vacancy, i.e., a model with the Ti^{3+} ion at the inequivalent titanium site along the [110] direction in Fig. 1(b) instead of one of the two equivalent titanium sites and thus in the same basal plane as the vacancy.

Our model of the $S = 1/2$ oxygen vacancy in rutile TiO_2 is illustrated in Fig. 11. The TiO_6 unit with the Ti^{3+} ion at the center and the oxygen vacancy at an equatorial position is shown in Fig. 11(a). Figure 11(b) is a projection on the (110) plane. It shows the Ti^{3+} ion and the four equatorial oxygen ions (one of which is the vacancy). The principal axes associated with the g_3, A_3, and Q_3 principal values are all along the [001] direction. Figure 11(c) is a projection on the (001) plane. In this view, the Ti^{3+} ion and the two apical oxygen ions are in the plane of the figure while the four equatorial oxygen positions (one being the oxygen vacancy) are above and below this plane. The principal axes associated with the g_1, g_2, A_1, and A_2 principal values are shown in Fig. 11(c). The Q_1 and Q_2 axes are nearly coincident with the A_1 and A_2 axes. We recognize that there will be some lattice relaxation associated with the $S = 1/2$ oxygen vacancy. However, there are presently no experimental results that allow us to determine the magnitudes and directions of displacements of the primary Ti^{3+} ion and the other neighboring titanium and oxygen ions from their regular unperturbed positions. It is expected that a detailed description of the lattice relaxation accompanying the $S = 1/2$ oxygen vacancy will emerge from future computational studies.

An interesting and important aspect of our EPR and ENDOR results is the disparity in the directions of the basal-plane principal axes of the **g** and hyperfine **A** matrices. As can be seen in Table I and Fig. 11(c), the g_1 and A_1 directions deviate by approximately 51.3°. It is typical for transition-metal ions to have the **g** and hyperfine principal axes coincide, especially when the paramagnetic ion occupies a site of high symmetry.[42] However, Pilbrow and Lowrey,[43] in their 1980 review, show that the **g** and **A** principal axes of transition-metal ions may have significantly different orientations when the symmetry at the metal ion is low. In our present case of an $S = 1/2$ oxygen vacancy, lattice relaxation will quite likely lower the symmetry at the Ti^{3+} ion and allow the **g** and **A** principal axes to be different. Pilbrow and Lowrey[43] suggest that the role of excited-state orbitals, under the influence of low-symmetry fields, is largely responsible for the different orientations of the principal directions. In addition to clarifying the nature of the lattice relaxation, future computational studies may also provide insight to the electronic structure (i.e., *d*-orbital mixture) of the ground state of the singly ionized oxygen

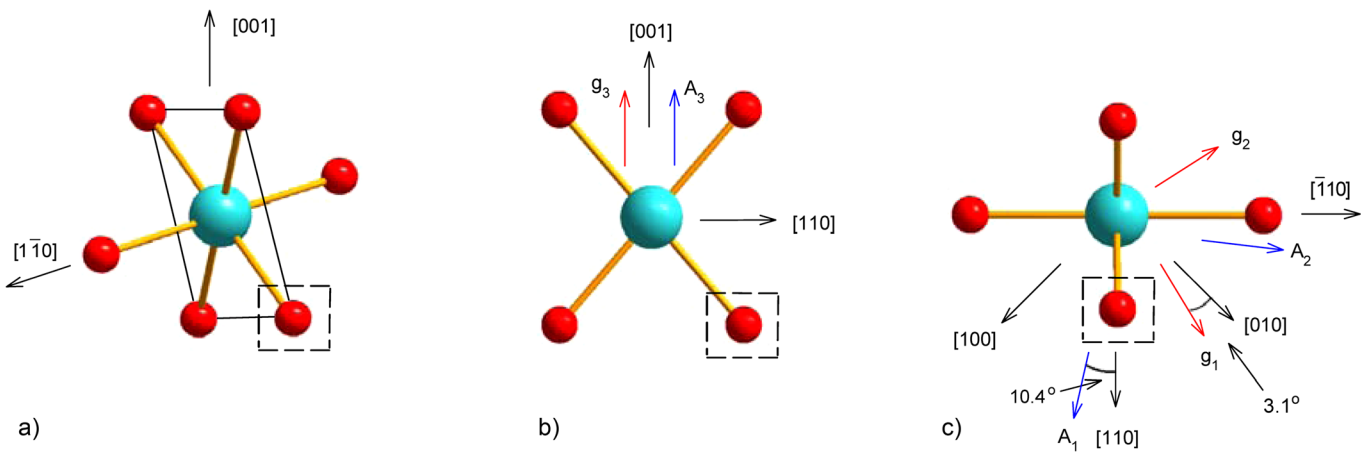

FIG. 11. Model of the singly ionized $S = 1/2$ oxygen vacancy in rutile TiO_2. (a) A three-dimensional view of a TiO_6 unit, showing the Ti^{3+} ion (blue) at the center and the oxygen vacancy (denoted by the dashed square) at one of the four equatorial positions. (b) A projection of the TiO_6 unit on the (110) plane. (c) A projection of the TiO_6 unit on the (001) plane showing the basal-plane principal-axis directions. In this last projection, the Ti^{3+} ion and the two apical oxygen ions are in the plane of the figure while the four equatorial oxygen positions (one being the oxygen vacancy) are above and below this plane.

vacancy in rutile TiO_2 crystals and help explain the differences in the **g** and **A** basal-plane principal-axis directions.

VI. SUMMARY

A detailed EPR and ENDOR investigation of the hyperfine structure associated with the $S = 1/2$ oxygen vacancy in the interior of a bulk rutile TiO_2 crystal shows that the unpaired spin in this defect is localized on one adjacent titanium ion (i.e., it is a Ti^{3+} ion adjacent to an "empty" vacancy). The experimental characterization of the ground state of this singly ionized donor includes measurements of the **g** matrix[10,11] and the ^{47}Ti and ^{49}Ti hyperfine and nuclear electric quadrupole matrices (**A** and **Q**). Principal-axis directions of the hyperfine and nuclear electric quadrupole matrices are nearly coincident, and differ significantly from the principal-axis directions of the **g** matrix. Extrapolating from the known structure of the closely related $S = 1$ neutral oxygen vacancy in bulk rutile TiO_2 leads us to propose a model for the $S = 1/2$ singly ionized oxygen vacancy that has the vacancy located at one of the equatorial oxygen positions next to the Ti^{3+} ion.

ACKNOWLEDGMENTS

One of the authors (A.T.B.) acknowledges support as a National Research Council Postdoctoral Fellow.

[1]X. Y. Pan, M. Q. Yang, X. Z. Fu, N. Z. Zhang, and Y. J. Xu, Nanoscale **5**, 3601 (2013).
[2]M. A. Henderson, Surf. Sci. Rep. **66**, 185 (2011).
[3]A. Fujishima, X. Zhang, and D. A. Tryk, Surf. Sci. Rep. **63**, 515 (2008).
[4]K. Szot, M. Rogala, W. Speier, Z. Klusek, A. Besmehn, and R. Waser, Nanotechnology **22**, 254001 (2011).
[5]J. J. Yang, M. D. Pickett, X. Li, D. A. A. Ohlberg, D. R. Stewart, and R. S. Williams, Nat. Nanotechnol. **3**, 429 (2008).
[6]G. Pacchioni, ChemPhysChem. **4**, 1041 (2003).
[7]M. Ménétry, A. Markovits, C. Minot, and G. Pacchioni, J. Phys. Chem. B **108**, 12858 (2004).
[8]S. Lany and A. Zunger, Phys. Rev. B **72**, 035215 (2005).
[9]S. Yang, L. E. Halliburton, A. Manivannan, P. H. Bunton, D. B. Baker, M. Klemm, S. Horn, and A. Fujishima, Appl. Phys. Lett. **94**, 162114 (2009).
[10]Shan Yang, "Paramagnetic resonance studies of defects in titanium dioxide crystals," Ph.D. dissertation (West Virginia University, Morgantown, WV, 2009).
[11]F. D. Brandão, M. V. B. Pinheiro, G. M. Ribeiro, G. Medeiros-Ribeiro, and K. Krambrock, Phys. Rev. B **80**, 235204 (2009).
[12]T. S. Bjørheim, A. Kuwabara, and T. Norby, J. Phys. Chem. C **117**, 5919 (2013).
[13]A. Janotti, C. Franchini, J. B. Varley, G. Kresse, and C. G. Van de Walle, Phys. Status Solidi (RRL) **7**, 199 (2013).
[14]P. Deák, B. Aradi, and T. Frauenheim, Phys. Rev. B **86**, 195206 (2012).
[15]H.-Y. Lee, S. J. Clark, and J. Robertson, Phys. Rev. B **86**, 075209 (2012).
[16]T. V. Perevalov and V. A. Gritsenko, J. Exp. Theor. Phys. **112**, 310 (2011).
[17]J. Stausholm-Møller, H. H. Kristoffersen, B. Hinnemann, G. K. H. Madsen, and B. Hammer, J. Chem. Phys. **133**, 144708 (2010).
[18]G. Mattioli, P. Alippi, F. Filippone, R. Caminiti, and A. A. Bonapasta, J. Phys. Chem. C **114**, 21694 (2010).
[19]B. J. Morgan and G. W. Watson, J. Phys. Chem. C **114**, 2321 (2010).
[20]S. G. Park, B. Magyari-Kope, and Y. Nishi, Phys. Rev. B **82**, 115109 (2010).
[21]C. Di Valentin, G. Pacchioni, and A. Selloni, J. Phys. Chem. C **113**, 20543 (2009).
[22]X. Li, M. W. Finnis, J. He, R. K. Behara, S. R. Philpot, S. B. Sinnott, and E. C. Dickey, Acta Mater. **57**, 5882 (2009).
[23]T. Minato, Y. Sainoo, Y. Kim, H. S. Kato, K. Aika, M. Kawai, J. Zhao, H. Petek, T. Huang, W. He, B. Wang, Z. Wang, Y. Zhao, J. Yang, and J. G. Hou, J. Chem. Phys. **130**, 124502 (2009).
[24]E. Finazzi, C. Di Valentin, G. Pacchioni, and A. Selloni, J. Chem. Phys. **129**, 154113 (2008).
[25]M. Chiesa, M. C. Paganini, S. Livraghi, and E. Giamello, Phys. Chem. Chem. Phys. **15**, 9435 (2013).
[26]S. Livraghi, M. Chiesa, M. C. Paganini, and E. Giamello, J. Phys. Chem. C **115**, 25413 (2011).
[27]S. Livraghi, S. Maurelli, M. C. Paganini, M. Chiesa, and E. Giamello, Angew. Chem., Int. Ed. **50**, 8038 (2011).
[28]A. M. Czoska, S. Livraghi, M. Chiesa, E. Giamello, S. Agnoli, G. Granozzi, E. Finazzi, C. Di Valentin, and G. Pacchioni, J. Phys. Chem. C **112**, 8951 (2008).
[29]M. Aono and R. R. Hasiguti, Phys. Rev. B **48**, 12406 (1993).
[30]S. Yang and L. E. Halliburton, Phys. Rev. B **81**, 035204 (2010).
[31]A. T. Brant, S. Yang, N. C. Giles, and L. E. Halliburton, J. Appl. Phys. **110**, 053714 (2011).
[32]A. T. Brant, N. C. Giles, and L. E. Halliburton, J. Appl. Phys. **113**, 053712 (2013).
[33]S. Yang, A. T. Brant, N. C. Giles, and L. E. Halliburton, Phys. Rev. B **87**, 125201 (2013).
[34]S. Watauchi, M. A. R. Sarker, M. Nagao, I. Tanaka, T. Watanabe, and I. Shindo, J. Cryst. Growth **360**, 105 (2012).
[35]S. C. Abrahams and J. L. Bernstein, J. Chem. Phys. **55**, 3206 (1971).
[36]C. J. Howard, T. M. Sabine, and F. Dickson, Acta Crystallogr., Sect. B: Struct. Sci. **47**, 462 (1991).
[37]K. H. Channappa and J. M. Pendlebury, Proc. Phys. Soc. **86**, 1145 (1965).
[38]H. Rinneberg and J. A. Weil, J. Chem. Phys. **56**, 2019 (1972).
[39]W. C. Tennant and R. F. C. Claridge, J. Magn. Reson. **137**, 122 (1999).
[40]M. M. Abraham, Y. Chen, L. A. Boatner, and R. W. Reynolds, Solid State Commun. **16**, 1209 (1975).
[41]A. M. Stoneham, *Theory of Defects in Solids* (Clarendon Press, Oxford) 1975, p. 465.
[42]A. A. Abragam and B. B. Bleaney, *Electron Paramagnetic Resonance of Transition Ions* (Clarendon Press, Oxford) 1970.
[43]J. R. Pilbrow and M. R. Lowrey, Rep. Prog. Phys. **43**, 433 (1980).